Applied Surface Science 255 (2008) 3414–3420

Contents lists available at ScienceDirect

Applied Surface Science

journal homepage: www.elsevier.com/locate/apsusc

Rolling and slipping motion of a water droplet sandwiched between two parallel plates coated with fluoroalkylsilanes

Shunsuke Suzuki [a,b], Akira Nakajima [a,b,*], Munetoshi Sakai [b], Ayako Hashimoto [b], Naoya Yoshida [b,c], Yoshikazu Kameshima [a,b], Kiyoshi Okada [a]

[a] Department of Metallurgy and Ceramic Science, Tokyo Institute of Technology, 2-12-1 O-okayama, Meguro-ku, Tokyo 152-8552, Japan
[b] Kanagawa Academy of Science and Technology, 308 East, Kanagawa Science Park, 3-2-1 Sakado, Takatsu-ku, Kawasaki-shi, Kanagawa 213-0012, Japan
[c] Research Center for Advanced Science and Technology, The University of Tokyo, 4-6-1 Komaba, Meguro-ku, Tokyo 153-8904, Japan

ARTICLE INFO

Article history:
Received 21 April 2008
Received in revised form 23 September 2008
Accepted 24 September 2008
Available online 4 October 2008

PACS:
Wetting (68.08.Bc), Liquid–solid interfaces (68.08.-p)

Keywords:
Wetting
Silane
Hydrophobicity
Coatings
Particle image velocimetry

ABSTRACT

Si plates were treated using two fluoroalkylsilanes (FAS17 and FAS3), and the internal fluidity of a water droplet sliding between two parallel plates on a slope was observed directly using particle image velocimetry (PIV) method with a high-speed camera system. The interfacial caterpillar-like rotation flows with slip motion at the solid–liquid interface were related to the combination of top and bottom wettabilities. The water droplets accelerated by a rolling and slipping motion on FAS17 coatings; the acceleration was dominated by a rolling motion on FAS3 coatings. A droplet's shape, solid–liquid molecular interaction, and the gravitic force will be important factors determining the sliding mode on a solid surface.

1. Introduction

Hydrophobic coatings have attracted much attention as an indispensable technology for production of various industrial items. A solid surface's hydrophobicity can be either of two types: static hydrophobicity or dynamic hydrophobicity [1]. The sliding angle (SA) (the critical angle at which a droplet starts sliding down an inclined surface by gradual tilting) and contact angle hysteresis (WCH) (the difference between the receding and advancing contact angles of a sliding droplet on an inclined surface) are often evaluated as criteria of dynamic liquid-repellency [2–5]. However, these criteria are insufficient to represent water-shedding kinetics such as sliding acceleration and the velocity of water droplets [1,6]. For surface material's design, information related to how fast the droplet can be removed from the surface at a certain tilt angle is becoming more important than that related to the lowest tilt angle at which the droplet slides downward. Recently, reports of the relation between surface properties and sliding velocity or acceleration are gradually increasing [7–10].

Very recently, we applied particle tracing velocimetry (PTV) and particle image velocimetry (PIV) to observe internal fluidity in water droplets during sliding on several hydrophobic silane coatings [8–10]. These studies revealed that water droplets slide down by a caterpillar-like rotation with or without slippage at the solid–liquid interface. Moreover, the rolling/slipping ratio depends on silane coatings' surface properties such as chemical homogeneity or surface roughness [10]. These results imply that dynamic hydrophobicity such as sliding velocity or acceleration depends strongly on internal fluidity.

On the other hand, the sliding behavior of water droplets surrounded by two or more hydrophobic surfaces has become important for cleaning electronic devices and designing industrial materials with droplets, such as fuel cells [11] and microelectromechanical systems (MEMS). During the last decade, hydrodynamics of liquids at a solid–liquid interface and confined by solid surfaces were investigated using several methods [12–19]. However, reports describing a water droplet sandwiched between parallel plates are few [20,21]. The sliding velocity (acceleration)

* Corresponding author.
E-mail address: anakajim@ceram.titech.ac.jp (A. Nakajima).

0169-4332/$ – see front matter © 2008 Elsevier B.V. All rights reserved.
doi:10.1016/j.apsusc.2008.09.059

and internal fluidity of the droplet during sliding between hydrophobic plates separated by millimeter-order distance on a tilted slope are not well understood.

In this study, a water droplet was sandwiched between two parallel Si plates that had been treated with fluoroalkylsilanes (FAS). We then used PIV method to evaluate the internal fluidity in the downward motion of water droplets. Then the contribution of slipping and rolling to the overall sliding acceleration of the droplet was examined.

2. Experimental

2.1. Sample preparation

A Si (100) wafer (*n*-type; Aki Corp., Miyagi, Japan) was cut into 3 cm × 5 cm plates and cleaned using acetone and water. Vacuum ultraviolet (VUV) light was irradiated (λ = 172 nm with a power density of around 7 mW cm^{-2}, UEM20-172; Ushio Inc., Tokyo, Japan) to the cleaned wafers for 10 min in air to form a homogeneous oxide layer [22,23]. For the present study, we used 1H,1H,2H,2H-perfluorodecyltrimethoxysilane (FAS17, $CF_3(CF_2)_7CH_2CH_2Si(OCH_3)_3$, TSL8233; GE Toshiba Silicones, Tokyo, Japan) and trifluoropropyltrimethoxysilane (FAS3, $CF_3(CH_2)_2Si(OCH_3)_3$, KBM7103; Shinetsu Chemical Co., Japan) as coating agents. The Si plates were set into a glass container with either 0.02 mL (FAS17) or 0.04 mL (FAS3) and sealed with a glass cap under dry N_2 conditions. Then, the container was heated in an oven to 423 K for 1 h (FAS17) or to 373 K for 3 h (FAS3). After that heat treatment, the plates' surfaces were rinsed using flowing toluene, acetone, and water; then they were dried at 353 K in air.

2.2. Evaluation of coatings

Surface roughness (R_a) was evaluated in a 5-μm-square area using atomic force microscopy (AFM, JSPM-5200; JEOL, Tokyo, Japan) with a Si tip (0.6 N/m spring constant). The static water contact angle (WCA) was measured using the sessile drop method with a 4 mg water droplet using a contact angle meter (Dropmaster 500; Kyowa Interface Science Co. Ltd., Saitama, Japan). Sliding angles and the advancing and the receding contact angles at the SA were measured for a 30-mg pure water droplet using a commercial system (SA-20; Kyowa Interface Science Co. Ltd.). Each measurement was performed at five different points for WCA and three points for SA, then averaged.

The droplet sliding behavior was observed directly by taking motion pictures using a high-speed camera system (100 or 1000 s^{-1} frame rate). A 30-μL droplet was prepared using a microsyringe on the sample surface, which was tilted at 35°; the droplet was triggered to slide by drawing the tip of the syringe. A CMOS camera with a 1024 × 1024 pixel sensor resolution (1024PCI; Photron Ltd., Tokyo, Japan) was used for taking images. The camera was rotated at 35° (slope inclination).

For PIV analysis, a 35 μL water droplet containing 0.06 mass% fluorescent particles (mainly polystyrene, 3 μm diameter, 1.05 cm^3 g^{-1} density; 542 nm excitation wavelength; 612 nm emission wavelength, R0300; Duke Scientific Corp., CA, USA) was prepared using a micropipette at the space between the plates. Hereinafter, we designate this suspension as the test-fluid. The two plates were set face-to-face on the slope with a space of 2.5 mm between the top and bottom surfaces. The sheet-shaped laser (Ar ion type, 1000 mW intensity; 488 and 514 nm wavelengths; ca. 200 μm width by the slit; Seika Corp., Tokyo, Japan) was emitted vertically to the interval space between these plates and was set to the center of droplet from the receding side during sliding. The arrangement of this sliding behavior evaluation system

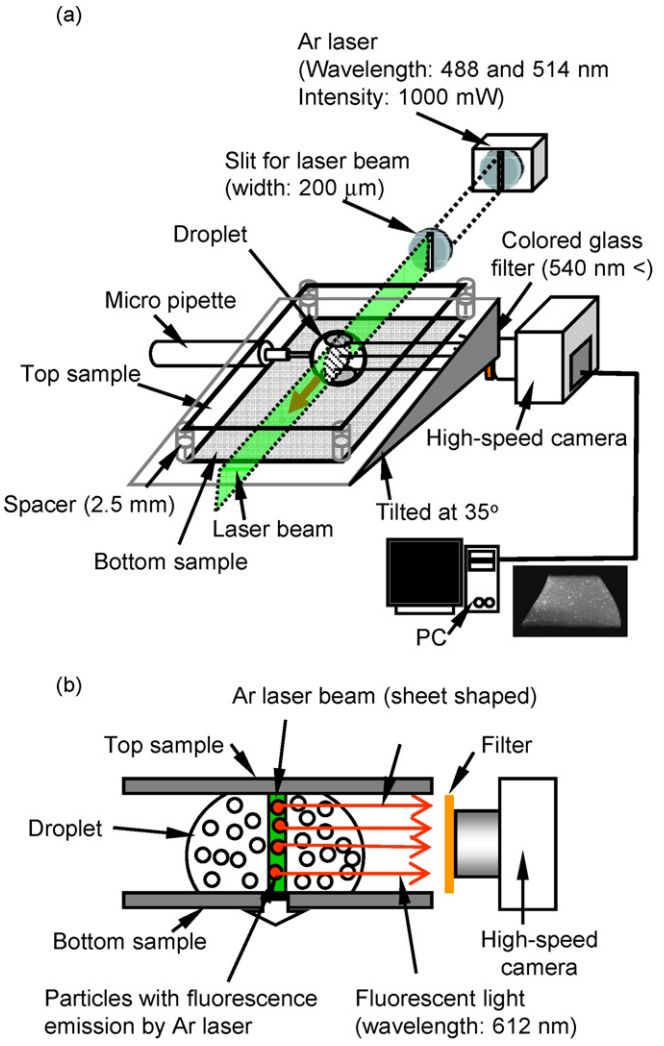

Fig. 1. Schematic diagram of the observation system. (a) Entire alignment for system and (b) detailed diagram for PIV analysis. A test-fluid droplet is sandwiched between two parallel plates on a tilted plane.

is presented in Fig. 1. Dynamic images of the excited particles were taken using the camera while filtering all other light sources. Immediately after starting to slide downward, the droplet vibrated for around 0.1 s. Therefore, we started evaluation at t = 0, when accidental deformation from the microsyringe tip had ceased. The sliding velocity and acceleration were evaluated for the edges on each contact line from the sliding distance using commercial software (DIP-Motion; Ditect Inc., Tokyo, Japan).

The internal velocity vector was evaluated using software (DIP-Flow-KAST; Ditect Inc., Tokyo, Japan) for the PIV method. Detailed techniques of this measurement were described in a previous study [9]. Briefly, it consists of tracking the peaks of the intensity cross-correlation of a PIV cells, which are from the meshed image of the droplet, at two different times. In our case, the cell size was 114 μm × 114 μm and the time separation was 10 ms (this value is 100 ms for the droplet sandwiched between FAS3 coatings). Each pixel was ca. 14 μm. Pattern matching for the image contrast of the cell was carried out for the area ±228 μm around the center of the cell using the correlation factor of 0.6. The distribution of the velocity vector on each cell was evaluated for the flow velocity. The wall areas of the top and the bottom surface were determined directly from the images.

The apparent surface energy of the test-fluid was measured using the pendant drop method with the contact angle meter.

Table 1
Averaged surface roughness (R_a), water contact angle (WCA), sliding angle for a water droplet (SA), and contact angle hysteresis (WCH) on prepared hydrophobic coatings.

	R_a (nm)	WCA (°)	SA (°)	WCH (°)
FAS17	0.22	107 ± 1	10 ± 1	13
FAS3	0.14	77 ± 1	13 ± 1	11

Viscosity was evaluated using an E-type viscometer (TVE-22LT; Toki Sangyo Co. Ltd., Tokyo, Japan) at 20 °C.

3. Results and discussion

3.1. Static and dynamic hydrophobicity of each coating

The surface roughness, water contact angle, sliding angle, and contact angle hysteresis recorded for advancing and receding contact angles at the sliding angle for FAS17 and FAS3 plates are presented in Table 1. Measurements made using AFM revealed that surfaces (R_a values were less than 1 nm) were smooth, with no dust or aggregation. The FAS17 coating shows a higher WCA and smaller SA than FAS3 does. The advancing and the receding contact angles were, respectively, 116 ± 1° and 103 ± 1° for FAS17, and 80 ± 2° and 69 ± 2° for FAS3.

The surface energy and viscosity of the test-fluid were, respectively, 70 mJ m^{-2} and 1.05 mPa s^{-1}. These are almost equivalent to the values for pure water. We confirmed that a droplet of pure water exhibits almost identical sliding velocity as the test-fluid droplet. Fig. 2 shows the sliding distance (d) of the advancing edge of a test-fluid droplet on a FAS17 or FAS3 plate against time (without the top plate). In the present study, the position of the droplet was evaluated at the bottom advancing point. Therefore, the original point of the sliding distance, namely $d = 0$, was the position of the bottom advancing point of the droplet when $t = 0$. Line fitting was carried out using the root mean square method. The droplet can slide down with acceleration on the FAS17 plate: the value was 6.8 × 10^2 mm s^{-2}. On the FAS3 plate, it was ca. 0 mm s^{-2}. The droplet's shape was almost constant in this area.

3.2. Dynamic hydrophobicity and internal fluidity of test-fluid droplets sandwiched between parallel coatings

Fig. 3 shows the sliding velocity of the droplet against time (t) for the sliding direction (x direction) of the advancing edge on the bottom plates of a 35-μL test-fluid droplet sandwiched between the two parallel plates of FAS17(top)–FAS17(bottom), FAS17–FAS3, FAS3–FAS17, and FAS3–FAS3. All droplets nearly retained their shape during sliding from d (distance) = 0–1.25 mm. The times necessary to reach $d = 1.25$ mm for a test-fluid droplet in FAS17(top)–FAS17(bottom), FAS17–FAS3, FAS3–FAS17, and FAS3–FAS3 combinations are, respectively, 0.14, 0.58, 0.40, and 2.1 s. The solid line represents the fitted lines by root mean square method. The droplet slid down with a higher acceleration when the bottom wall had a FAS17 coating.

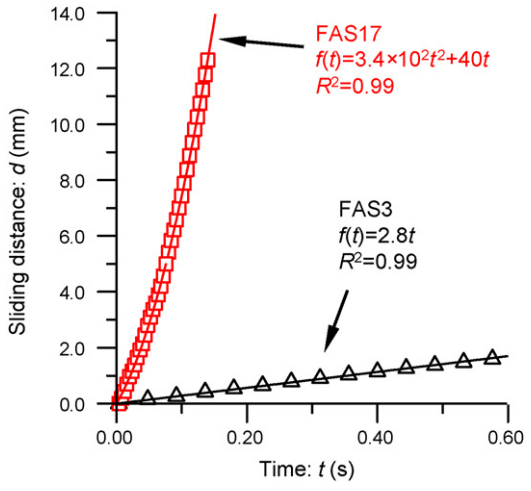

Fig. 2. Sliding distance, shown against time (t), of the advancing edge of a 35-μL-test-fluid droplet on a Si plate coated with FAS17 or FAS3.

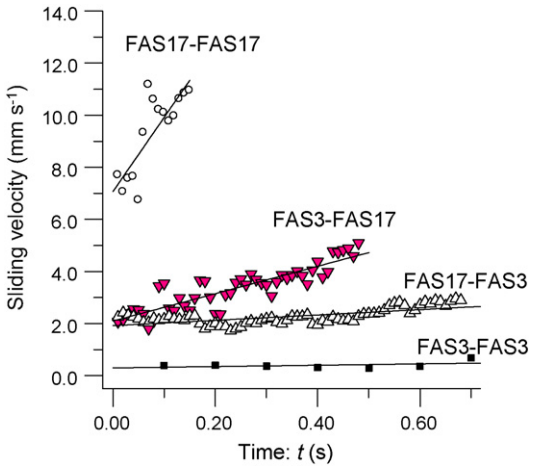

Fig. 3. Sliding velocity of the advancing edges on the bottom wall against time (t) for a test-fluid water droplet (35 μL) sliding between two parallel plates.

Fig. 4 shows the distribution of velocity vector evaluated using PIV analysis for each cell in the sliding test-fluid droplet between two plates at $d = 1.25$ mm. The z_{line} is parallel to the z-axis and passing the center of the droplet (see Fig. 5). This position was obtained by assuming a trapezoidal shape whose edges are at the advancing and receding edges on the top and bottom contact lines. The PIV cells around the middle height between the two plates exhibits higher velocity than the cells around the wall surfaces. Arranging the FAS3 coating in the system, the velocity values tended to decrease.

Fig. 6(a–d) show the vertical distribution curves of sliding velocity for the x direction (v_x) evaluated for PIV cells on each z_{line} for respective plate combinations. The position in which velocity vector took the highest values did not coincide with the center of the plates. The velocity curves depend not only on the chemical composition (FAS17 or FAS3) but also on the plate alignment (top or bottom).

Fig. 7 presents a schematic model of a droplet sliding between two parallel plates by the combination of models for each single plate (top and bottom plates). The velocity distribution in Fig. 6 resembles Poiseuille flow; the modeling to obtain sliding and slipping components from this velocity distribution is not established. We evaluated these components by assuming the linear velocity distribution model as the first approximation. The velocity distribution of the droplet sliding on hydrophobic silane coatings becomes linear in the early stage of sliding [9,10]; this assumption is applicable in such case. Between the plates, a sandwiched droplet advances by an interfacial caterpillar-like rotation flow with slippage at each solid–liquid interface. Here, A_T, A_B, R_T, and R_B all present advancing and receding edges of a contact line of the droplet. The respective sliding velocities of these edges are v_A, v_R, v'_A, and v'_R for the x direction (where $'$ means bottom side). These sliding velocities must be identical when the droplet deformation is negligible during sliding. The interfacial flows meet at the position of z_{max}, whose sliding velocity (v_{max}) is the highest

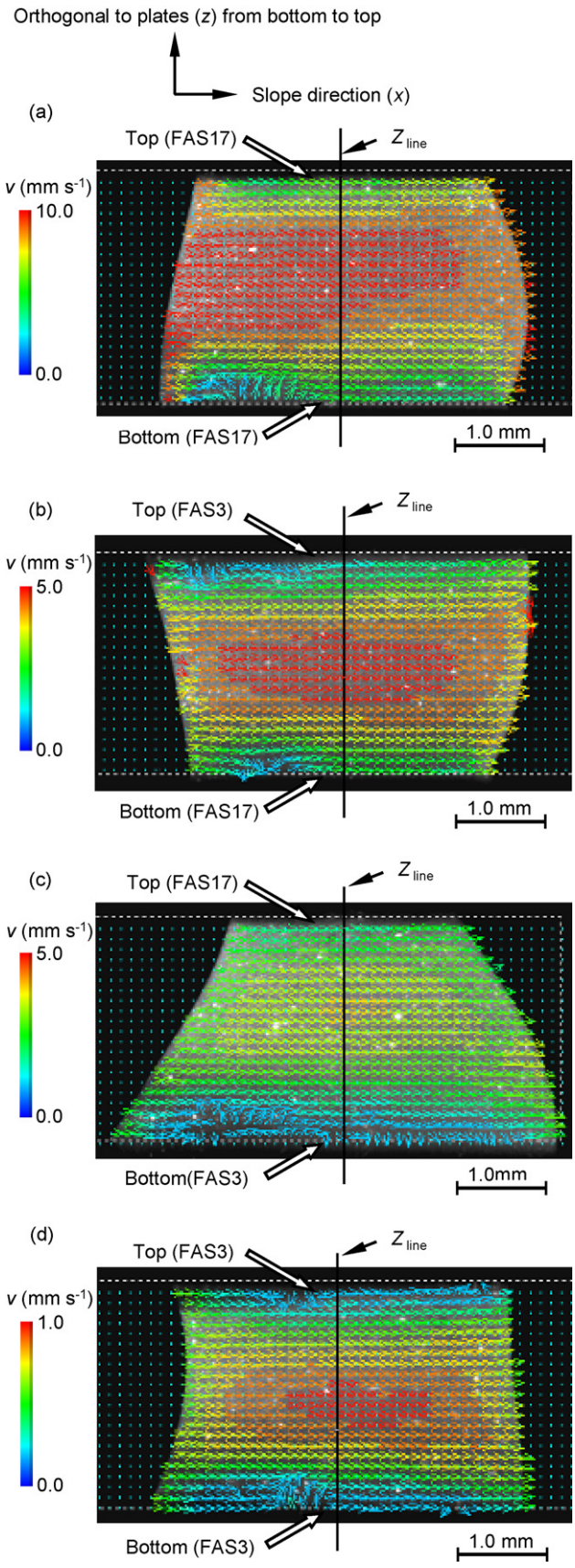

Fig. 4. Distribution of the velocity vector of the internal fluidity evaluated from PIV analysis for the test-fluid droplet sliding between two parallel Si plates with FAS17 and FAS3 coatings at d = 1.25 mm: (a) FAS17(top)–FAS17(bottom), (b) FAS3–FAS17, (c) FAS17–FAS3, and (d) FAS3–FAS3.

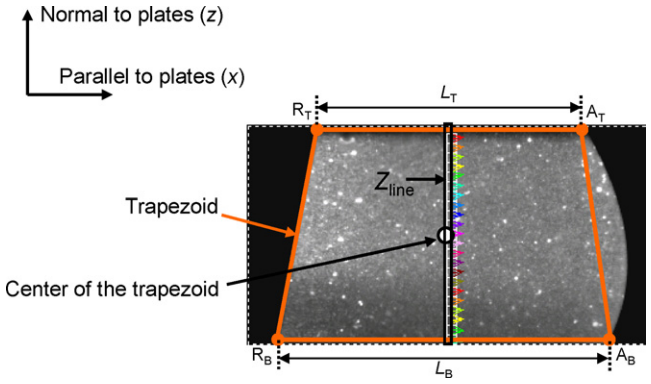

Fig. 5. PIV image of the droplet and determination of the z_{line} using the center position of a trapezoid, which edged at respective contact edges (A_T, A_B, R_B, and R_T) during sliding.

value on the z_{line}. In this study, the sliding velocities of slipping (v_{slip}) and rolling (v_{roll}) for the x direction were evaluated using the model portrayed in Fig. 7 from results of PIV analysis. As in previous studies [9,10], the "v_{slip}" value was obtained from the cell (size is 114 μm square) just on the surface. The rolling velocity for the x direction (v_{roll}) was evaluated using the following equation.

$$v_{roll} = \frac{v_{max} - v_{slip}}{2}$$

Table 2 shows the v_{slip} and v'_{slip} evaluated for a 35-μL droplet at d = 1.25 mm between each top and bottom surface. The FAS17 surface showed a higher slipping velocity than the FAS3 surface.

Figs. 8 and 9 respectively show the time dependence of evaluated v_{slip}, v'_{slip}, v_{roll}, and v'_{roll} for a 35-μL test-fluid droplet between FAS3(top)–FAS17(bottom) and FAS17–FAS3. In the observed region, those velocities increased almost linearly with time. The dotted and solid lines in the figures present the approximated lines using root mean square method. It is noticeable that FAS17 shows higher slipping velocities and a larger slope of approximated lines for them than FAS3. On FAS3 (especially for the case of the bottom of FAS3), the rolling velocity became higher than the slipping one, which suggests that large friction of slippage was avoided by the rolling mechanism on the FAS3 surface. A similar trend was obtained from the combinations of FAS17–FAS17 and FAS3–FAS3.

Table 3 shows sliding acceleration of a 35-μL test-fluid droplet on each plate in a sandwiched system. In this study, sliding acceleration ($a_{droplet}$) was evaluated by averaging the sliding accelerations of A_T, A_B, R_T, and R_B. Their respective standard deviations were also calculated for motion of these edges. Using PIV analysis for each plate surface and root mean square method, a_{slip} and a_{roll} were evaluated from the time-dependence of v_{slip}, v'_{slip}, v_{roll}, and v'_{roll}, as shown in Figs. 8 and 9. Similarly to the single plate case, the expected sliding acceleration of droplet (a_{calc}) was evaluated as a summation of a_{slip} and a_{roll}. They were almost equal to the actual sliding acceleration ($a_{droplet}$) measured from the sliding distance of the droplet edges, suggesting that the modeling and evaluation of each element remained appropriate for the

Table 2
The slipping velocity of 35-μL water droplet at top surface (v_{slip}) and bottom surface (v'_{slip}) evaluated at d = 1.25 mm.

(Top)–(Bottom)	v_{slip} (mm s^{-1})	v'_{slip} (mm s^{-1})
FAS 17–FAS17	5.6	4.0
FAS3–FAS17	0.8	2.0
FAS17–FAS3	1.6	0.1
FAS3–FAS3	0.2	0.1

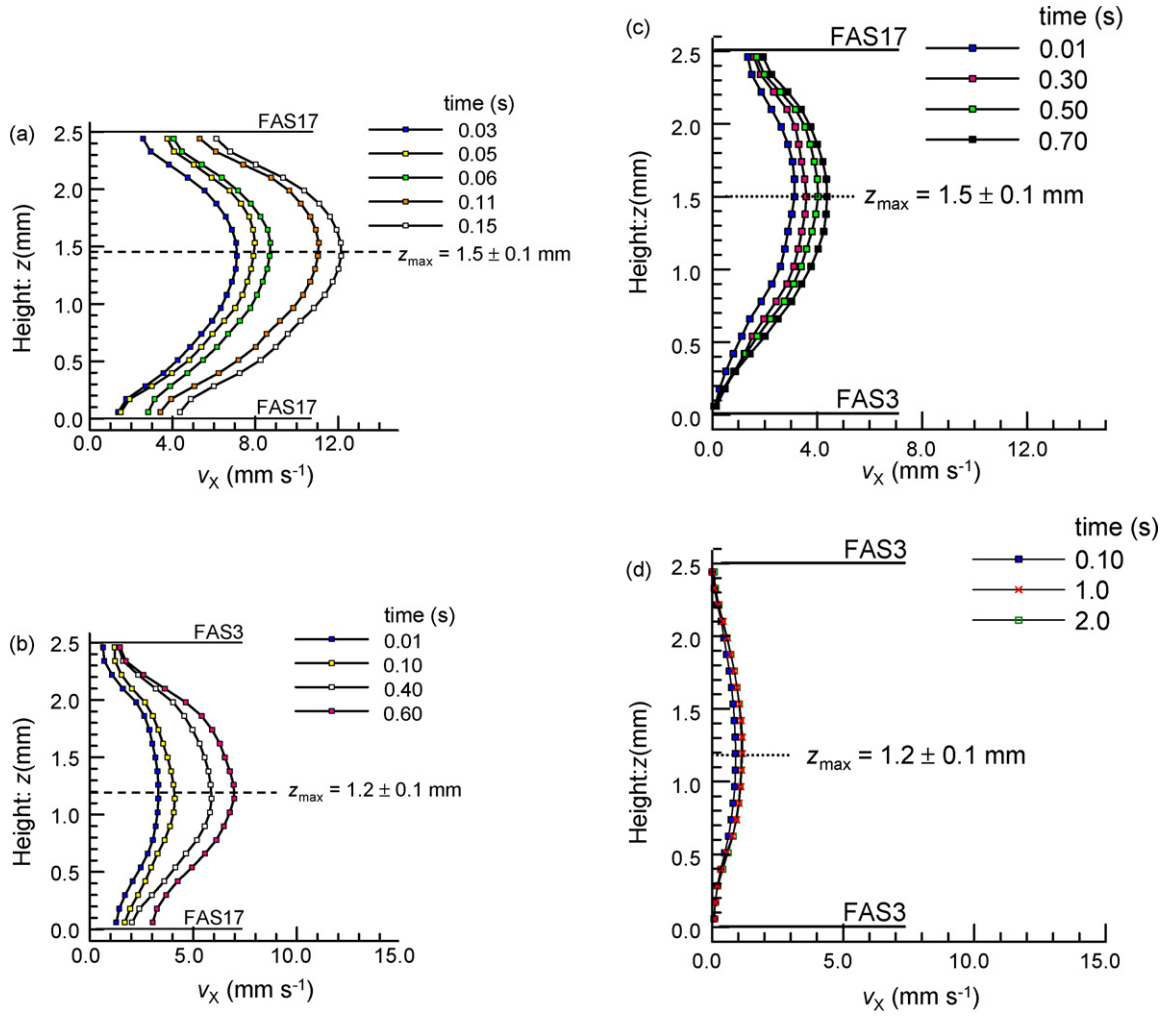

Fig. 6. Sliding velocity profiles on the z_{line} evaluated from PIV analysis against z position in a test-fluid droplet sliding between (a) FAS17(top)–FAS17(bottom), (b) FAS3(top)–FAS17(bottom), (c) FAS17(top)–FAS3(bottom), and (d). FAS3(top)–FAS3(bottom).

sandwiched system, as developed from the combination of single plate model [9,10]. Moreover, it suggests that effects of surface curvature of droplets and scattering or reflection of emitted light are almost negligible. The discrepancy of around 20% between the calculated acceleration (a_{calc}) and actual acceleration ($a_{droplet}$) in Table 3 might be attributable to the assumption of linear velocity distribution. Detailed analysis for a Poiseuille-like flow is a subject that will be addressed in future work.

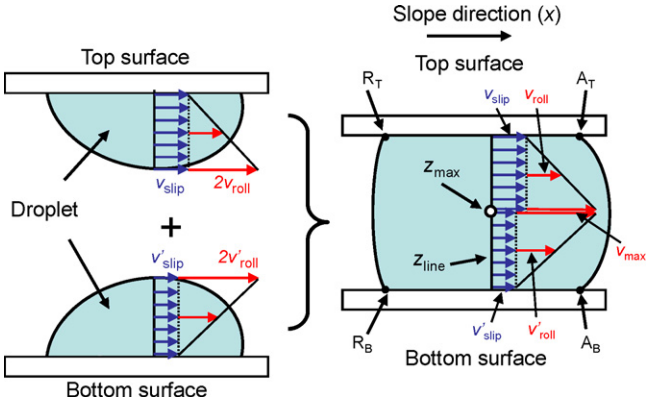

Fig. 7. Schematic illustration of the internal fluidity model in a droplet sliding on single plates (top and bottom) and between them.

The ratios between rolling and slipping component (a_{slip}/a_{roll}) for each plate surface are listed in the table as $R_{slip/roll}$. The values of $R_{slip/roll}$ are higher for the surface treated with FAS17. On the other hand, the rolling ratio on sliding acceleration is higher on the FAS3 surface. This result shows that the liquid can accelerate the velocity by increasing both the rolling and the slip velocities on FAS17 surface, whereas a rolling motion mainly governs the acceleration of the water droplet on FAS3. The droplet slides by a caterpillar-like rotation to avoid the large friction with slippage at the solid–liquid boundary [10]. The a_{slip} and a_{roll} evaluated in this study indicate that the FAS3 coating presents greater difficulty for sliding with a slip motion than FAS17, probably because it engenders a stronger interaction between the water and the solid surface than FAS17.

In the confined test-fluid droplet, the flow condition at one side plate affects that at the other side plate: the sliding velocity of the whole droplet can decrease when either of the plates has a lower slip velocity. Additionally, the gravitic force can increase the solid–liquid interaction at the bottom wall. It is noteworthy that the slip acceleration on the bottom FAS17 wall in FAS3–FAS17 (a_{slip} = ca. 2.6 mm s^{-2}) is higher than that on the top FAS17 plate in FAS17–FAS3 (a_{slip} = ca. 1.5 mm s^{-2}).

The magnitude of the slip velocity at the boundary must be affected by the solid–liquid interaction. Surface heterogeneities and

Table 3
Comparison of each sliding acceleration for sandwiched system between FAS17 and FAS3.

(Top)–(Bottom) acceleration	FAS17–FAS17		FAS3–FAS17		FAS17–FAS3		FAS3–FAS3	
	Top	Bottom	Top	Bottom	Top	Bottom	Top	Bottom
$a_{droplet}$ (mm s^{-2})	32 ± 3		5.3 ± 1.4		2.7 ± 0.8		~0	
a_{slip} (mm s^{-2})	22	19	1.1	2.6	1.5	0.1	~0	~0
a_{roll} (mm s^{-2})	7.7	9.3	2.7	1.9	0.9	1.6	~0	~0
a_{calc} (mm s^{-2})	37	38	6.5	6.4	3.3	3.3	~0	~0
$R_{slip/roll}$	2.9	2.0	0.41	1.4	2	0.1	–	–

the surface energy of coatings are expected to affect the slipping motion at the solid–liquid boundary. Derek et al. and Doshi et al. reported the possibility of the depletion of liquid molecules at the nonwetting solid wall and the existence of gaseous phase between the solid–liquid boundaries [24,25]. Those results provide a possible explanation of the different sliding behaviors of FAS3 and FAS17. Moreover, the dissipation of such a depression layer under the pressured condition might explain the effects of gravitic force in a sandwiched system on sliding behavior. However, it remains unclear whether such a depletion layer and vapor phase can be maintained at the boundary under large dynamics of water molecules in droplet sliding. Another plausible explanation is the long-range interaction between water and the substrate (SiO_2 and SiOH can be considered). The molecular lengths of FAS17 and FAS3 are evaluated respectively as ca. 1.33 and 0.42 nm [22]. Even the attractive van der Waals force extends a few nanometers from the substrate; Coulombic interaction extends a greater distance. Such a long-range interaction implies that the interaction from Si substrate to water molecules differs between FAS3 and FAS17. Moreover, a difference in the freedom of rearrangement is reported for different CF moiety [26]. Further

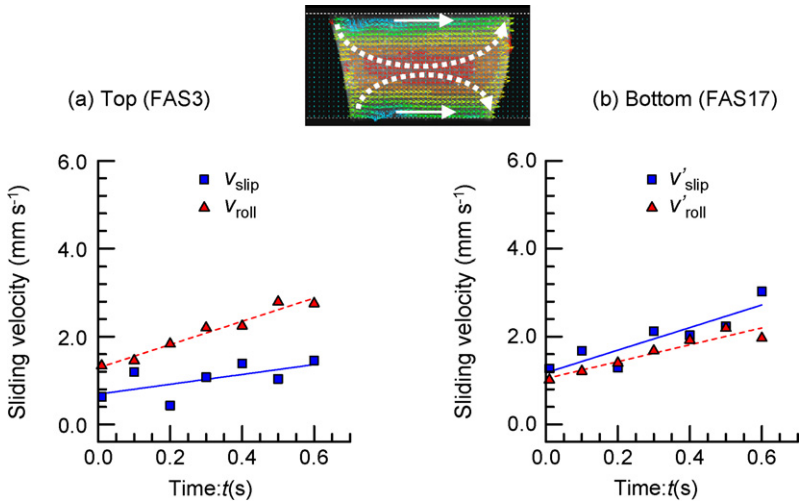

Fig. 8. Time dependence of slipping and rolling velocities for the *x* direction of a 35-μL test-fluid droplet between FAS3(top) and FAS17(bottom). (a) At the top surface and (b) at the bottom surface.

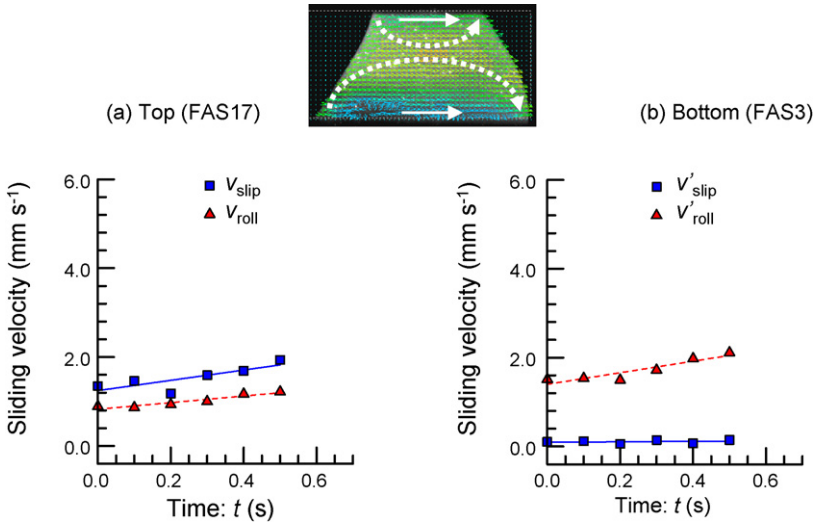

Fig. 9. Time dependence of slipping and rolling velocities for the *x* direction of a 35-μL test-fluid droplet between FAS17(top) and FAS3(bottom). (a) At the top surface and (b) at the bottom surface.

experiments with various solid surfaces and computing simulations would be helpful to explore slip phenomena on silane coatings.

4. Conclusion

In this study, the internal fluidity in a water droplet sliding between two parallel plates treated with different fluoroalkylsilanes was evaluated using PIV analyses. The obtained images revealed that water droplets slid down with interfacial rotation flows and slipping motion at the solid–liquid interface. These rates depended on the combination of chemical compositions of the top and the bottom walls. A water droplet can accelerate on the FAS17 coating with increases in both the rolling velocity and slipping velocity, although it accelerated on the FAS3 coating mainly by the rolling velocity. The gravitic force increased the slipping velocity on the top wall and decreased it on the bottom wall. Interfacial rotation flows and slip conditions of the water droplet were determined not only by surface conditions of one side wall, but also by that of the other side. Control of the sliding behavior of a water droplet and its dominant sliding mode (rolling mode and/or slip mode) can be realized by changing the combination of the top and the bottom walls with silane coatings.

References

[1] A. Nakajima, J. Ceram. Soc. Jpn. 112 (2004) 533.
[2] A. Carre, M.E.R. Shanahan, J. Adhesion 49 (1995) 177.
[3] E. Wolfram, R. Faust, in: J.F. Padday (Ed.), Wetting, Spreading, and Adhesion, Academic Press Inc., London, 1978 (Chapter 10).
[4] J.P. Youngblood, T.J. McCarthy, Macromolecules 32 (1999) 6800.
[5] H. Murase, K. Nanishi, H. Kogure, T. Fujibayashi, K. Tamura, N. Haruta, J. Appl. Polym. Sci. 54 (1994) 2051.
[6] N. Yoshida, Y. Abe, H. Shigeta, A. Nakajima, H. Ohsaki, K. Hashimoto, T. Watanabe, J. Am. Chem. Soc. 178 (2006) 743.
[7] S. Suzuki, A. Nakajima, Y. Kameshima, K. Okada, Surf. Sci. 557 (2004) 163.
[8] M. Sakai, J.-H. Song, N. Yoshida, S. Suzuki, Y. Kameshima, A. Nakajima, Langmuir 22 (2006) 4906.
[9] M. Sakai, A. Hashimoto, N. Yoshida, S. Suzuki, Y. Kameshima, A. Nakajima, Rev. Sci. Inst. 78 (2007) 045103.
[10] S. Suzuki, A. Nakajima, M. Sakai, Y. Sakurada, N. Yoshida, A. Hashimoto, Y. Kameshima, K. Okada, Chem. Lett. 37 (2008) 58.
[11] Z. Zhigang, X. Jinsheng, Mu Pan, Y. Runzhang, J. Power Sources 160 (2006) 1.
[12] R. Pit, H. Hervet, L. Léger, Phys. Rev. Lett. 31 (2000) 980.
[13] D.C. Tretheway, C.D. Meinhart, Phys. Fluids 14 (2002) L9.
[14] C. Cottin-Bizonne, S. Jurine, J. Baudry, J. Crassous, F. Restagno, É. Charlaix, Eur. Phys. J. E 9 (2002) 47.
[15] T. Schmatko, H. Hervet, L. Léger, Langmuir 22 (2006) 6843.
[16] C.-H. Choi, K. Johan, A. Westin, K.S. Breuer, Phys. Fluids 15 (2003) 2897.
[17] B.-Y. Cao, M. Chen, Z.-Y. Guo, Phys. Rev. E 74 (2006) 066311.
[18] J. Xu, Y. Li, J. Inter, Heat Mass Trans. 50 (2007) 2571.
[19] P. Joseph, P. Tabeling, Phys. Rev. E 71 (2005), 035303(R).
[20] K. Suzuki, Y. Uyeda, Tribo. Lett. 15 (2003) 77.
[21] K. Suzuki, Microsyst. Technol. 11 (2005) 1107.
[22] A. Hozumi, K. Ushiyama, H. Sugimura, O. Takai, Langmuir 15 (1999) 7600.
[23] H. Sugimura, K. Ushiyama, A. Hozumi, O. Takai, Langmuir 16 (2000) 885.
[24] C.T. Derek, D.M. Carl, Phys. Fluids 14 (2002) L9.
[25] D.A. Doshi, E.B. Watkins, J.N. Israelachvili, J. Majewski, PNAS 102 (2005) 9458.
[26] K. Honda, M. Morita, H. Otsuka, A. Takahara, Macromolecules 38 (2005) 5699.